Hidden magnetism in periodically modulated one dimensional dipolar fermions

Journal of Electroanalytical Chemistry 1008 (2026) 119915

Contents lists available at ScienceDirect

Journal of Electroanalytical Chemistry

journal homepage: www.elsevier.com/locate/jelechem

A Pseudo one dimensional model to describe the kinetic limitations in lithium–sulfur batteries

Tommaso Filippo Lupatelli [a,*], Massimo Santarelli [a], Silvia Bodoardo [b], Daniele Versaci [b]

[a] Synergy of Thermo-chemical and Electro-chemical Power Systems (STEPS), Department of Energy, Polytechnic of Turin, corso Duca degli Abruzzi 24, 10129 Turin, Italy

[b] Electrochemistry Group, Department of Applied Science and Technology, Polytechnic of Turin, corso Duca degli Abruzzi 24, 10129 Turin, Italy

ARTICLE INFO

Keywords:
Pseudo one dimensional
Lithium sulfur
Mass transport
Deposition kinetic
Potentiostatic electric impedance spectroscopy

ABSTRACT

In the latest years Lithium sulfur batteries (Li—S) have reached a wide interest in the research field as suitable candidate as post Lithium-ion batteries, due to their high theoretical specific capacity and potentially lower cost. However, their practical implementation is still hindered by several challenges principally related to the intrinsic chemistry of such system. Here is proposed a new modelling approach, a pseudo-one-dimensional (P1D) modelling framework is employed to investigate the role of polysulfides transport and precipitation kinetics as sources for reversible capacity losses, while guaranteeing low computational cost and avoiding mesh implementation. The model is parameterized on a CR2032 coin cell and validated against experimental discharge data over a broad current range, starting from 0.1C up to 1C. The model faithfully reproduces the characteristic two-plateau discharge profile and the supersaturation point associated with peak internal resistance. Providing a capacity reduction above 250[$mAhg^{-1}$], primarily affecting the second voltage plateau, by increasing the current rate from 0.1C to 1C. Correlating the accumulation of intermediate polysulfides within the separator at high rates to reversible capacity losses, with concentrations up to five times higher compared to lower discharge rates. The framework discussed allows also to highlight the relationship between electrolyte viscosity, $Li_2S_{(s)}$ precipitation kinetics, and internal resistance at different current intensity. Simulating an increase of the internal resistance of almost 50%, coupled also with a shift of the peak respect the state of discharge. The results proved the ability of the model to describe one of the major issues of lithium sulfur battery highlighting, at microscale level, its contribution on the precipitation kinetic, resistivity and its influence on the C-rate.

1. Introduction

In the latest years lithium–sulfur (Li—S) batteries have emerged as one of the most promising alternatives to conventional lithium-ion (Li-ion) technologies in order to supply a constant growing demand of clean and sustainable energy. Their major advantage lies in their exceptionally high theoretical energy density, approaching 2500$\left[WhKg^{-1}\right]$ [1–4], which is significantly higher than that of currently commercially available Li-ion cells. The high theoretical energy density of the sulfur cathode, 1675$\left[mAhg^{-1}\right]$ [5], coupled with a lithium metal anode, makes Li—S batteries a serious alternative as light weight energy device, suitable for aerospace and electric vehicles [6]. Moreover, sulfur (S_8) is an abundant, inexpensive and environmental friendly material making the Li—S chemistry an attractive candidate from both economic and sustainability perspectives, with the potential to develop low cost energy system exceeding 500[$Whkg^{-1}$] [7–9] in the future. However, despite their advantages, Li—S batteries face several challenges that have so far hindered their commercialization.

The most critical issue is the rapid capacity fading over repeated cycles, due to the so-called “shuttle phenomenon”, involving the long soluble chain polysulfides which are soluble into the electrolyte and can move freely inside the cell, reaching the lithium anode where they can reduce and precipitate on top of the electrode surface as insulating species, leading to both capacity loss and degradation of the solid electrolyte interphase (SEI) [10,11]. Nevertheless, severely advances and new approach has been made regarding metal-anode protection [12,13]. Furthermore, the conversion chemistry of sulfur cathode leads during discharge a volume change up to 80%, with detrimental consequence on the conductive matrix and the contact with the current collector [14,15]. Lastly both sulfur and its discharge products are electric insulators, which can precipitate on the cathode surface, reducing the

* Corresponding author.
E-mail address: tommaso.lupatelli@polito.it (T.F. Lupatelli).

https://doi.org/10.1016/j.jelechem.2026.119915
Received 17 December 2025; Received in revised form 7 January 2026; Accepted 2 February 2026
Available online 4 February 2026

Nomenclature

Symbols

C_i	Concentration of the dissolved species i
$C_{i,ref}$	Reference concentration of the dissolved species i
ε	Porosity
r_j	Reaction rate for the electrochemical reaction j
R_j	Reaction rate for the non-faradaic reaction j
$D_{i,eff}$	Effective diffusive coefficient for the species i
d	Bruggeman coefficient
σ_{ele}	Electrolyte ionic conductivity
R_{ele}	Electrolyte ionic resistivity
σ_{pos}	Cathode electric conductivity
R_{pos}	Cathode electric resistivity
$\sigma_{pos,i}$	Electric conductivity of the solid fraction i
$E_{j,ref}$	Open circuit potential for the electrochemical reaction j
$E^0_{j,ref}$	Standard Open circuit potential for the electrochemical reaction j
i^0_j	Activation current for the electrochemical reaction j
$i^0_{ref,j}$	Reference activation current for the electrochemical reaction j
η_j	Activation overpotential for the electrochemical reaction j
n_j	Electron exchanged in the reaction j
a^0_v	Initial value of specific surface area
a_v	Specific surface area for electrochemical reaction
F	Faraday constant
T	Temperature
R	Gas constant
A	Geometric area of the cell
N_i	Flux for species i
z_i	Charge species i
I	Applied current

overall electric conductivity and increasing over polarization.

In the latest years, several efforts have been made to overcome these issues, using different carbon matrix, from doped graphene structure [16] or 3D porous matrix [17], in order to encapsulate as much as possible the sulfur within the cathode structure, reducing shuttling and at the same time sulfur utilization.

Regardless of the efforts made, the challenges mentioned above and the complex chemistry still represent a significant problem for future development and commercialization of Li—S batteries. In this scenario continuum modelling has become an essential tool in order to provide a wider understating and to accelerate the progress of Li—S batteries [18,19]. Inside continuum modelling a microscale approach can be used in order to break down each individual reaction step, focusing on the kinetic and transport processes that govern Li—S batteries to an elementary level, focusing on the kinetic of polysulfides conversion and diffusion within the computational domain. Such model scale provides a framework for quantifying and predicting the evolution of key species within the battery, offering a valuable insight into how design parameters and operating conditions affect performance and lifetime. One of the earliest significant contributions to the theoretical modelling of Li—S batteries was proposed by Mikhaylik et al. [20], which developed a zero dimensional, 0D or lumped, model that captured the charge and discharge characteristics across different current densities, using a simplified two reaction scheme. The model qualitative matches the typical discharge profile of a Li—S battery, however, underestimate the complex chemistry and the kinetic within the cell, such as the role of polysulfides diffusion. Although, their work represents a first step for understanding the electrochemical behavior of Li—S systems, using a low computational expensive approach.

Kumaresan et al. [21] proposed a more extensive and physically detailed one-dimensional (1D) model that included a multi-step sulfur reduction scheme. Their approach divided the solid sulfur, $S_{8_{(s)}}$ to S^{2-} conversion into five distinct electrochemical reactions, each corresponding to the formation and consumption of intermediate polysulfide species. Furthermore, their model accounts also for the precipitation and dissolution of four solid lithium polysulfides, including their role in the porosity evolution and, consequently, on the diffusion of dissolved species following a Bruggeman approach. However, their model has been discussed as not properly suitable to capture properly intrinsic behavior of Li—S batteries. In fact, even though, Kumaresan model stands as breakdown approach in the field of continuum modelling of Li—S batteries, as later studies [22,23] have pointed out, it does not fully capture the sensitivity of Li—S battery behavior to mass transport phenomena. Moreover, the model is based on 1D approach, making it more computationally demanding.

The diffusivity of polysulfides plays a critical role in the capacity delivered, leading to the introduction of reversible capacity loss, dependent on the current intensity. At high current densities, diffusion-limited transport of active species leads to inhomogeneous concentration gradients, which shift the dissolved species far from the cathode, making the separator a sink/source of active material. Zhang coupled experimental and modelling approach to understand the role of the current intensity on the capacity delivered, highlighting the role of the limited kinetic of polysulfides diffusion within the computational domain, as source of reversible capacity loss [22]. Through modelling, it was proved that, at low current, the concentration profiles inside the cathode and at the anode separator interface were more homogenous. This is due to the mismatch between the electrochemical reduction and the diffusion, which is a significantly slower phenomenon, and therefore at smaller current intensity is less impactful, allowing the polysulfides to diffuse back in the cathode. Overall, the work of Zhang and *co*-authors proved that the diffusivity of polysulfides plays a critical role in the capacity delivered, leading to the introduction of reversible capacity loss, depending on the current intensity.

Nevertheless, Zhang model was developed in a 1D framework, making it more consuming from a computational perspective. While it is able to describe a microscale process, such as the role of mass transport on the capacity delivered, it completely neglects other phenomena, as the evolution of the electrolyte viscosity and the cathode structure dependences on the state of discharge [24–26]. Experimentally, several studies using different approaches have proved that the internal resistance of the cell significantly changes during discharges, reaching a maximum at the supersaturation point [26–29]. The internal resistance can be simplified as sum of two major contributions: the electrolyte viscosity and the cathode electric conductivity, both highly dependent on the SOD ([%]). To explore these phenomena, Zhang et al. [30] proposed a process based on five electrochemical pathways for sulfur reduction and a single precipitation/dissolution reaction for $Li_2S_{(s)}$, treated as a non-Faradaic reaction. Their model focused primarily on the role of Li^+ ion concentration on the electrolyte viscosity, and its effect on voltage loss. Li^+ion was considered as and the main contributor to the evolution of electrolyte conductivity, as it can be assumed reasonably as the most relevant species present during all discharge process, reaching a concentration several order of magnitude higher than the other dissolved species. The model was validated using experimental data obtained through potentiostatic electrochemical impedance spectroscopy (PEIS), to detect the evolution of internal resistance as function of the SOD ([%]). This model has been proved valuable for capturing a crucial

process in Li—S behavior with relatively low computational cost: However, due to its inherent lack of spatial resolution, it is not suitable to account for local concentration gradients or mass transport limitations, which are essential key to understanding performance under realistic operating conditions. Furthermore, the model neglects the contribution of insulating species on overall internal resistance.

In this paper, a pseudo-one-dimensional approach (P1D) was implemented to provide a simplified model framework capable of describing the role of limited kinetic polysulfide diffusion as a source of reversible capacity loss, without the need to introduce any space-dependent equation, thereby reducing overall computational cost. The novelty approach here proposed consists of exploiting the inhomogeneity presents within a Li—S battery during discharge, simplifying the modelling domain in two distinct regions, the anode-separator interphase and the porous cathode. These two regions are treated as single points being able to exchange dissolved species and therefore mass. Li^+ ions are continuously generated by the metal anode, meanwhile they are consumed by $Li_2S_{(s)}$ deposition at the cathode. The mass transport of dissolved species and $Li_2S_{(s)}$ deposition are both phenomena characterized by a way slower kinetics in comparison to any of the electrochemical activities involved. Due to these kinetic discrepancies, the effect of such processes on the overall performances is highly dependent on the current intensity applied. Particularly, the diffusion of dissolved polysulfides between the separator and the porous cathode is mainly responsible for the reduced capacity delivered at high currents intensity. The P1D framework aims to implement such limitations in Lithium Sulfur battery and at the same time to reduce the computational cost of the model, as it is needed to solve only seven ordinary differential equations, ODE, for each domain. Nevertheless, the model here proposed has been proven to capture the relationship between reversible capacity losses ad current intensity, similarly to the model proposed by Zhang et al. [22], without needing to solve any PDE or account for the migration contribution derived from the electrolyte potential. Furthermore, in this study is addressed the role of $Li_2S_{(s)}$ deposition at high current density, aiming to characterize the kinetic mismatch between non faradaic reactions and the electrochemical process, focusing especially on its role as source of voltage losses. The model framework was used in a wide range of current densities and deposition kinetics, demonstrating its flexibility and capability to cover several processes simultaneously. Lastly, the evolution of the internal resistance of the cell was investigated as a function of the current density, with a particular focus to the contribution of both the electrolyte and the cathode structure. The model proved a strong dependance between the ohmnic drop and the current rate, crucial in conversion system as Lithium Sulfur batteries. In addition, the employed modelling framework allows to track the evolution of the major component of the internal resistance throughout the entire discharge, comparing and validating the model results against experimental data obtained by PEIS. The model here presented aims to provide an alternative approach for the investigation of mass transport phenomena without relying on PDE, while still allowing the evaluation of two interconnected domains. At the same time, the framework implemented can be considered a valuable tool to study the dependence of the system performance towards the applied electrochemical conditions, a crucial aspect for conversion system as Lithium Sulfur batteries.

2. Model development

2.1. Model frameworks

The model is based on a pseudo one dimensional approach, positioned between a zero-dimensional (0D) and a one-dimensional (1D) scale, developed in COMSOL Multiphysics. It aims to describe the effects of active species diffusion within the electrolyte, which continuously move back and forward from the porous cathode, where the electrochemical reduction of polysulfides takes place. Typically, in 0D models the cell is modelled as a lumped system and therefore neglect any spatial variations, leading to the formation of concentration gradients of polysulfides within the electrolyte. Consequently, this class of model is unable to capture the role of diffusion as source of reversible capacity loss, as previously highlighted by Zhang et al. [22]. On the contrary, by incorporating the effects of concentration gradients, the pseudo-dimensional model, similarly to a 1D model, can describe the role of diffusion and its effect on the cell performance without considering the spatial dependence of each variable or implementing a geometrical mesh. Inside the P1D model was only considered the effect of Fick diffusion, generated by concentration gradient between the two domains in analysis. This substantially reduces both computational cost and simulation time. Furthermore, as pointed out by Parke et al. [16] in their review on continuum modelling, in order to provide a more accurate description of the discharge profile and to capture the various contributions to overpotential losses, the model needs to consider additional aspects. For this reason, our model includes the impact and evolution of electrolyte viscosity, which directly influences ionic mobility and transport resistance, as well as the dynamic processes of precipitation and dissolution of sulfur species within the porous cathode structure, and their effects on the electric conductivity.

2.2. Electrochemical/chemical reactions

During discharge, the solid sulfur, $S_{8(s)}$, is gradually dissolved into the electrolyte as dissolved sulfur $(S_{8(l)})$ which is successively electrochemical reduced to lower order polysulfides, following a complex multistep reaction pathway. Several reaction schemes can be used to describe the electrochemical conversion of sulfur [20,31–33], guaranteeing both accuracy and simplicity. First it was assumed that the solid $S_{8(s)}$ volume fraction does not contribute to any electrochemical reaction, meanwhile the dissolved $S_{8(l)}$ is reduced according to the following scheme:

$$\frac{1}{2}S_{8(l)} \leftrightarrow \frac{1}{2}S_8^{2-} \tag{1}$$

$$\frac{3}{2}S_8^{2-} \leftrightarrow 2S_6^{2-} \tag{2}$$

$$S_6^{2-} \leftrightarrow \frac{3}{2}S_4^{2-} \tag{3}$$

$$\frac{1}{2}S_4^{2-} \leftrightarrow S_2^{2-} \tag{4}$$

$$\frac{1}{2}S_2^{2-} \leftrightarrow S^{2-} \tag{5}$$

This approach it was firstly introduced by Kumaresan et al. [21] allowing a deeper description of the Li—S conversion chemistry. In particular, during discharge, $S_{8(l)}$ is gradually reduced into soluble polysulfides following five different steps, meanwhile, at the anode side, the Li metal is oxidized according to Eq. 6:

$$Li \leftrightarrow Li^+ + e^- \tag{6}$$

Li—S performance is characterized not only by the reduction chain of sulfur, but also by non-faradaic reactions, which are strongly influenced by the used electrolyte formulation. First, the concentration of $S_{8(l)}$ changes not only as a consequence of the electrochemical reactions, but also for the gradual dissolution of solid sulfur inside the electrolyte:

$$S_{8(s)} \leftrightarrow S_{8(l)} \tag{7}$$

Furthermore, it is theoretically necessary to account for the solubility limit of each dissolved polysulfide, which leads to the precipitation of $Li_2S_{(s)}$ as insoluble insulating products on the porous carbon surface,

Table 1
Transport properties and Reference concentrations.

Specie (i)	z_i	$D_{i,0}\,(m^2 s^{-1})$	$C_{i,ref}\,(mol m^{-3})$
Li^+	1	0.88e−11	1100
$S_{8(l)}$	0	0.88e−13	19
S_8^{2-}	−2	3.5e−13	0.18
S_6^{2-}	−2	3.5e−12	0.32
S_4^{2-}	−2	1.75e−12	0.02
S_2^{2-}	−2	0.88e−12	5.23e−6
S^{2-}	−2	0.88e−12	8.27e−8

Table 2
Kinetic and thermodynamic properties [30].

Reaction (j)	$i_{j,0,ref}\,(A m^{-2})$	$E_{j,0,ref}\,(V)$
1	2	2.38
2	1.5	2.24
3	1	2.15
4	0.6	2.05
5	0.3	1.94
6	Xx	0

consequently affecting the electrode structure and its electrochemical performance. However, according to several studies [33–35], only $Li_2S_{(s)}$ can be considered as major deposition species, and its formation can be expressed according to eq. 8:

$$2Li^+ + S^{2-} \leftrightarrow Li_2S_{(s)} \tag{8}$$

2.3. Governing equations

The purpose of the P1D model is to describe the diffusion of active species between the cathode and the separator, considering only the effect of concentration gradient, without implementing migration contribution due to the electrolyte potential gradient. The electrochemical reduction of sulfur typically occurs within the cathode, meanwhile, the separator can be considered as both reservoir and source for polysulfides. During discharge, a concentration unbalance between these two domains generates a flux of dissolved species. At the beginning the concentration mismatch shift the polysulfides towards the separator, until the unbalance is reversed in favour of the cathode, due to electrochemical activity. The mass balance for each variable can be summarized in the equation below, where $r_{j,i}$ is the electrochemical reaction rate for the specific reaction j and $R_{k,i}$ stands for the non-faradaic contribution coming from the precipitation/dissolution reaction j: (Table 1)

$$\frac{d(\varepsilon C_i)}{dt} = -D_{i,eff}\frac{\Delta C_i}{l^2} + r_{j,i} + R_{k,i} \tag{9}$$

$$D_{i,eff} = D_i{}^*\varepsilon^d \tag{10}$$

2.4. Kinetics and equilibrium potential

The relationship between the current intensity for each specific electrochemical reaction *j* and the overpotential is expressed through Butler-Volmer equation, assuming that the anodic and cathodic charge transfer coefficients are equal to 0.5:

$$i_j = 2i^0_{j,ref} sinh\left(\frac{n_j F}{2RT}\eta_j\right) \tag{11}$$

The current intensity for the reaction j is dependent on the reference activation current (reported in Table 2), the gas kinetic constant and the temperature. Lastly the total applied current I is set as a boundary for the total volumetric current exchange within the cathode domain, which depends on the available active surface a_v and the geometrical properties of the cell, such as the cross-section A and the cathode thickness l_{pos}:

$$a_v \sum_j i_j = \frac{I}{A l_{pos}} \tag{12}$$

$$a_v = a^0_v \left(\frac{\varepsilon}{\varepsilon_0}\right)^6 \tag{13}$$

(See Table 3.)

Concerning the open circuit voltage, the Nernst voltage equation is implemented, accounting for the concentration of each dissolved species C_i involved in the electrochemical reaction j respect the reference concentration. A correction factor of 1000 is applied to convert moles per litre to moles per unit:

$$E_{j,ref} = E^0_j - \frac{RT}{n_j F}\sum\nolimits_i s_{i,j} ln\left(\frac{c_{i,ref}}{1\,[mol\,L^{-1}]}\right) \tag{15}$$

For simplicity, the formation of Li^+ was assumed to be ideal, hence any correlated overpotential can be neglected [28]. Therefore, the generation rate of Li^+ derives directly from the charge balance conservation, in order to compensate the reduction of sulfur at the cathode:

$$r_{Li^+} = \frac{a_v}{F}\sum_j i_j \tag{16}$$

2.5. Kinetics for non faradaic reactions

As mentioned above, during discharge, $S_{8(s)}$ is gradually dissolved into S_8(l) inside the electrolyte:

$$R_{S_8(s)} = k_{S_{8(s)}}\varepsilon_{S_{8(s)}}\left(C_{S_{8(s)}} - K_{sp,S_8}\right) \tag{17}$$

The precipitation of insoluble polysulfide species is considered only for the final product, $Li_2S_{(s)}$. The precipitation rate depends on the solid volume fraction of already deposited $Li_2S_{(s)}$, as implemented by Kumaresan et al. [22], to address the effect of a slower kinetic at the beginning of the discharge, and its linearly proportional to the kinetic constant $k_{Li_2S(s)}$:

$$R_{Li_2S(s)} = k_{Li_2S(s)}\varepsilon_{Li_2S_{(s)}}\left([C_{Li^+}]^2\left[[C_{S^{2-}}] - K_{sp,Li_2S}\right)\right. \tag{18}$$

The evolution of the free porous volume within the cell during the discharge is described Through the precipitation rate of the non-faradaic reaction, where V_k is the molar volume for the solid fraction k:

$$\frac{d\varepsilon}{dt} = -\sum_k V_k R_k \tag{19}$$

For simplicity it was assumed that non-Faradaic reactions can occurs only within the porous cathode domain.

Table 3
Precipitation kinetics parameters.

Precipitate (k)	Rate constant(k_k)	Solubility Product ($k_{sp,k}$)	Molar Volume V_k $(m^3 mo l^{-1})$
$S_{8(s)}$	$5[s^{-1}]$	$19[molm^{-3}]$	256.56
$Li_2S_{(s)}$	1.5e-4$\left[m^6 mol^2 s^{-1}\right]$	1e3$[mol^3 m^{-9}]$	45.95

Table 4
Electric properties of solid/liquid phase.

Phase	Symbol	Conductivity (Sm^{-1})
Electrolyte	$\sigma_{ele,0}$	6.8e−2
$S_{8(s)}$	$\sigma_{S_{8(s)}}$	5e−14
$Li_2S_{(s)}$	$\sigma_{Li_2S_{(s)}}$	10e−13
Ketjenblack EC − 300*JD*	σ_{KJB}	1000

Table 5
Geometrical parameters.

Parameter	Value
l	$50e-6[m]$
l_{pos}	$25e-6[m]$
A	$1.76e\text{-}4[m^2]$
a_v	$1.5e5[m^{-1}]$
ε_{S_8}	0.155
ε_{KJB}	0.11
ε_{Li_2S}	1e−7

2.6. Internal resistance evolution

It has been experimentally observed that the cell resistivity is highly dependent on the SOD. In addition, it has been demonstrated that the electrolyte cannot be treated as an ideal solution. In fact, the gradual increase of Li^+ causes an increase of viscosity leading to a reduction of the ionic conductivity until the supersaturation point. Then, due to the precipitation, the conductivity returns closer to its initial value. To describe this dependency a linear relationship between the electrolyte conductivity and the cation concentration was followed, furthermore the porosity of the cathode ε was also added to account for the effect of non-faradaic reactions:

$$\sigma_{ele} = \varepsilon\left(\sigma_{ele,0} - b\left(C_{Li^+} - C_{Li^+_{ref}}\right)\right) \tag{20}$$

$$R_{ele} = \frac{l\sigma_{ele}}{A} \tag{21}$$

During discharge, the internal structure of the cathode undergoes continuous changes due to the dissolution of elemental sulfur and the precipitation of lithium sulphide ($Li_2S_{(s)}$), both of which are electronically insulating materials. This dynamic transformation leads to a continuous variation in the effective electrical conductivity of the cathode. Even if such phenomena have been incorporated in several 1D models these are typically implemented using the Bruggeman-type correction, where the effective conductivity is assumed to depend exclusively on the volume fraction of the solid phase, without considering its specific chemical composition [34,35]. In the present approach, the electric conductivity was defined as a production factor of the conductivity of each specific species (reported in Table 4), and their solid fraction at a specific SOD([%]), following the relationship:

$$\sigma_{pos} = \prod \sigma_{pos,i}^{f_i} \tag{22}$$

$$R_{pos} = \frac{l\sigma_{pos}}{A} \tag{23}$$

Lastly, the cell voltage can be simply expressed as the difference

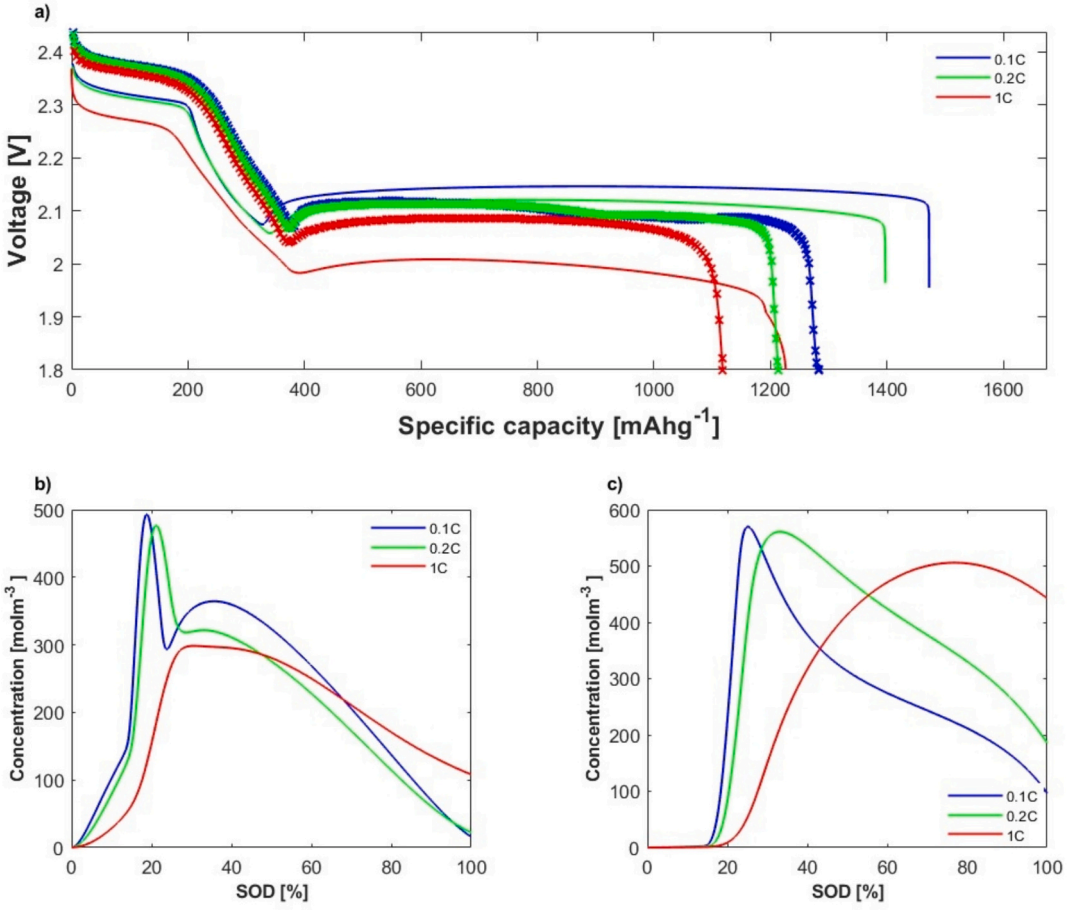

Fig. 1. Rate capability comparison of the P1D model: a) Voltage profile vs specific capacity for the three cases in analysis compared with experimental results b) S_6^{2-} concentration inside the separator vs SOD [%] c) S_4^{2-} concentration inside the separator vs SOD [%].

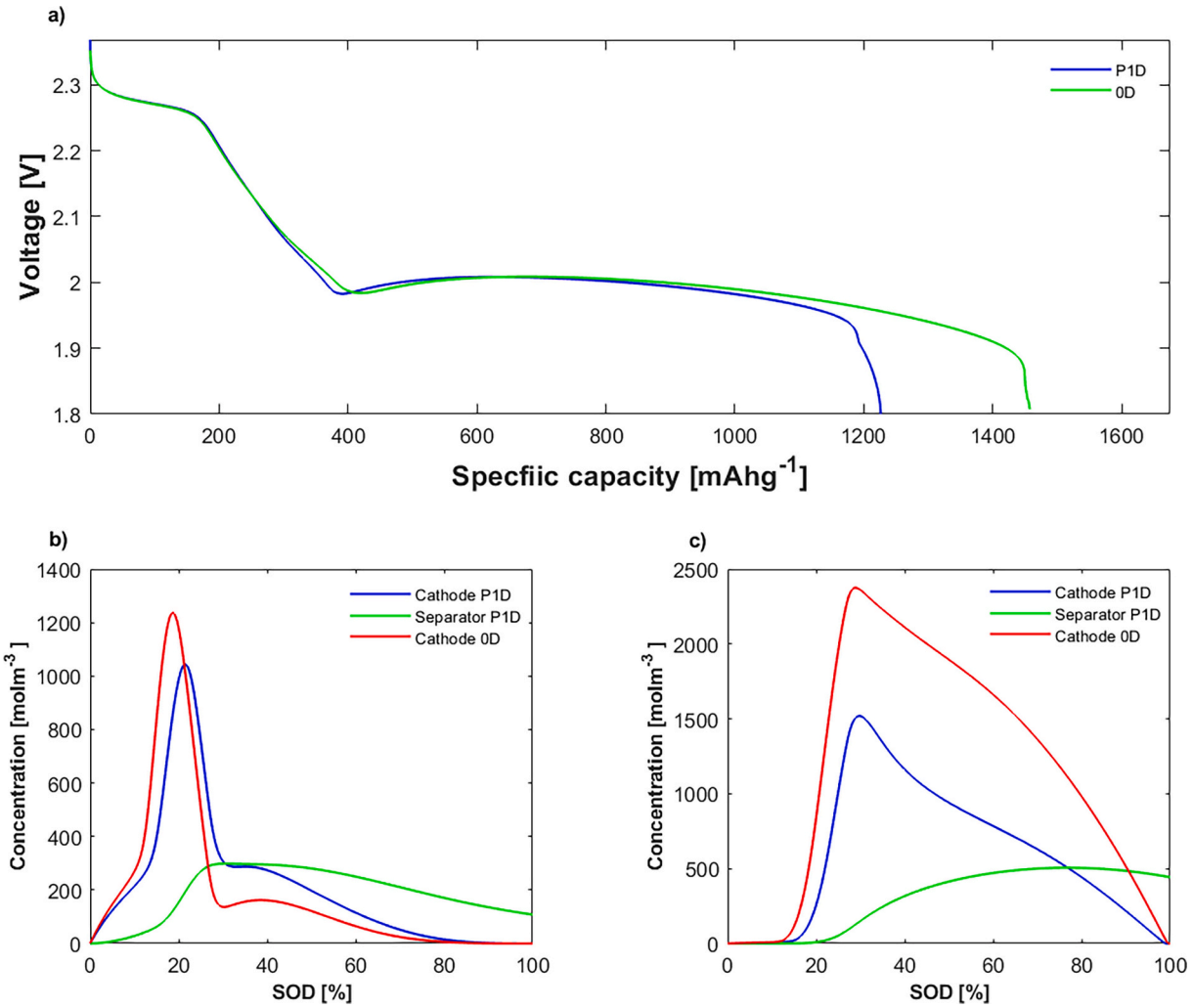

Fig. 2. Comparison between a P1D and an 0D model at 1C: a) Voltage profile vs specific capacity at 1C b) S_6^{2-} concentration inside the domains vs SOD [%] c) S_4^{2-} concentration inside the domains vs SOD [%].

between the equilibrium potential and the ohmic drops taking into account also the activation overpotential for the sulfur reduction:

$$V_{cell} = E_{j,ref} + \eta_j - E_{Li,ref} - (R_{ele} + R_{pos}) * I \quad (24)$$

3. Results and discussion

3.1. Polysulfides limited kinetic

The cell was modelled based on a coin cell CR2032, with all relevant details concerning the electrode manufacturing process and the cell assembling reported in the Supporting Information. The theoretical capacity of the cell used in the model is 2.61 mAh, corresponding to an initial solid sulfur mass of 1.56 mg. The geometrical properties and composition of the cell are summarized in Table 5.

Fig. 1a shows the predicted specific discharge capacity at various current rates, 0.1C, 0.2C and 1C, which were considered more suitable for results comparison. The simulated cells were also compared with experimental results, represented with marked lines, obtained from coin cells with same properties as reported in Table 5 and tested under same currents intensity, all the details are reported in the supporting information. From the confront can be proven the ability of the model faithfully reproduce the typical discharge profile of a Li—S battery, including the higher voltage plateau associated with the reduction of high-order polysulfides, a supersaturation point corresponding to the peak in cell resistivity, and a lower-voltage plateau related to the formation of intermediate and low-order polysulfides. As the current rate increases, the voltage profile shifts downward due to higher overpotential losses, related to both activation and ohmic contributions. In addition, can a slight shift of the supersaturation point at higher capacity can be clearly observe, as previously reported in the model proposed by Mistry et al. [36]. Our modelling framework approach has been proven reliable in describing the reduction of the delivered capacity as a function of the C-rate, due to the limited kinetic of polysulfide diffusion, a phenomenon reported both experimentally and through modelling by Zhang et al. [22].

As observable in Fig. 1a, the capacity mostly affects the second voltage plateau, while the first plateau is not severely affected. Indeed, as the current increases, the overall contribution follows a similar trend, starting 23% of the capacity delivered at 0.1C and 32% at 1C. The differences between simulation and modelling results can be partially attributed to experimental errors and uncontrolled factors occurring along the entire process, from electrode fabrication to cell assembly, which hinder the complete utilization of sulfur, consequently leading to a reduction of the capacity delivered. Nevertheless, the model successfully reproduces the magnitude of the capacity decay with increasing current density, thereby demonstrating good fidelity to the experimental behavior. The reduction in capacity delivered is primarily attributed to the inability of polysulfides to move sufficiently fast between the cathode and the separator reservoir. The dissolved polysulfide species S_i

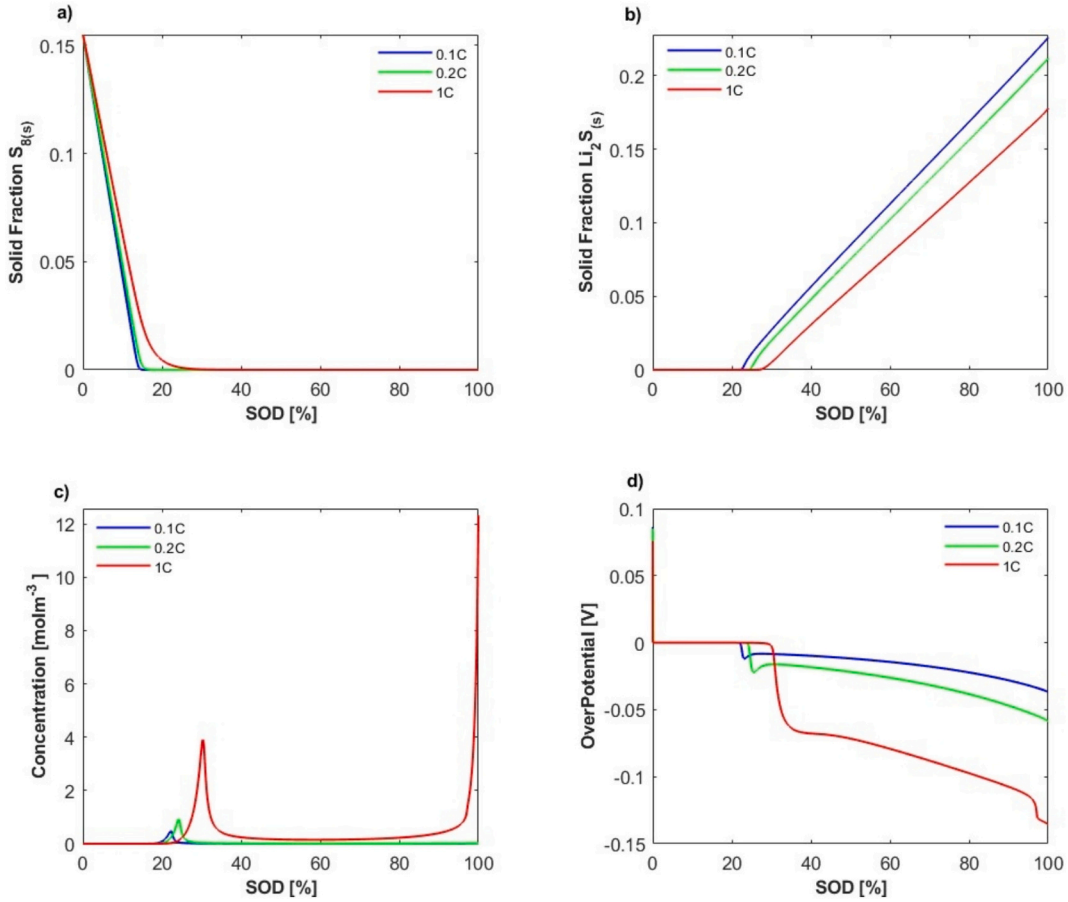

Fig. 3. Effect of the current intensity on the solid fraction evolution and losses: a) $S_{8(s)}$ fraction vs SOD [%]b) S_2^{2-} concentration inside the cathode vs SOD [%] c) $Li_2S_{(s)}$ fraction vs SOD[%] d) Activation overpotential η_5 vs SOD[%].

during discharge is shifted by the concentration unbalance towards the separator, until a favourable profile towards the cathode is formed, however due to kinetic limitations, a portion of polysulfides remain in the separator. Since diffusion is a far slower process in comparison with electrochemical reduction, at high C-rate the delayed transport of polysulfides become predominant, leading to reversible capacity loss. Fig. 1a clarifies the role of separator as sink for active material, showing that the concentration of S_6^{2-} and S_4^{2-} inside the separator increases as consequence of current rate. During discharge, the polysulfides move towards the separator due to a more favourable concentration gradient, before being attracted back to the cathode. However, the limited kinetic prevents a homogenous distribution, leading to residual dissolved species inside the separator, at the end of discharge.

To highlight the role of the limited kinetic of polysulfides diffusion, as source of reversible capacity loss, in Fig. 2a is reported a direct comparison between the P1D and a 0D model at 1C, coupled with the evolution of concentration of both S_6^{2-} and S_4^{2-} as function of the SOD ([%]). As previously discussed, diffusion limitations have minimal impact on the first discharge plateau but significantly reduce the second, resulting in a notable loss in deliverable capacity. As polysulfides are generated during discharge, a concentration gradient is generated, driving their diffusion from the cathode towards the separator. When the driving force is reversed, due to the limited kinetics, these species cannot return efficiently to the reaction zone, effectively reducing the accessible capacity.

Therefore, this reversible loss mechanism results from the residual polysulfides which remain in the separator at the end of discharge. In contrast, the 0D model does not include any spatially resolved transport effects, hence is not able to capture this diffusion-limited loss. As a result, 0D model typically provides a higher sulfur utilization, unrealistically independent from the current intensity and kinetic limitations [18].

The limited kinetic of Li—S batteries is not only related to polysulfide diffusion, but also to non faradaic reactions, which control the evolution of the solid fraction inside the cell, and therefore directly affecting both transport properties and electrochemical activity. Figs. 3 reports the concentration of both S_8 and $Li_2S_{(s)}$vs the SOD ([%]). From Fig. 3a it is evident as the current intensity increases, the dissolution rate of solid sulfur is not sufficiently fast to keep up with the electrochemical reduction. As a result, the model shows a delayed sulfur dissolution relative to the overall state of discharge, which leads to a shift of the supersaturation point. A parallel delay is also visible for the deposition of $Li_2S_{(s)}$, which starts above 30% of the SOD ([%]). This results in a lower overall solid fraction at the end of the discharge, highlighting the dependencies between the C-rate and precipitation kinetic, as previously verify through modelling [37].

In general, the influence of $Li_2S_{(s)}$ precipitation kinetics on overall cell performance has been widely discussed in the literature, using an electrochemical approach [31] or describing the process as a chemical reaction [21,30,32]. In our model a simplified approach was used, following a chemical description of $Li_2S_{(s)}$, mainly focusing on the effect of kinetic inhomogeneity as source of capacity loss. In particular, in comparison to the model proposed by Zhang et al. [30] which investigated the limited kinetic of $Li_2S_{(s)}$only in a limited current range (0.03–0.15C), the present model extends the range up to 1C. As can be seen in Fig. 3b, the concentration of S^{2-} dissolved in the electrolyte, within the porous cathode domain, depends on the applied current intensity. The increase of S^{2-} begins around the supersaturation point,

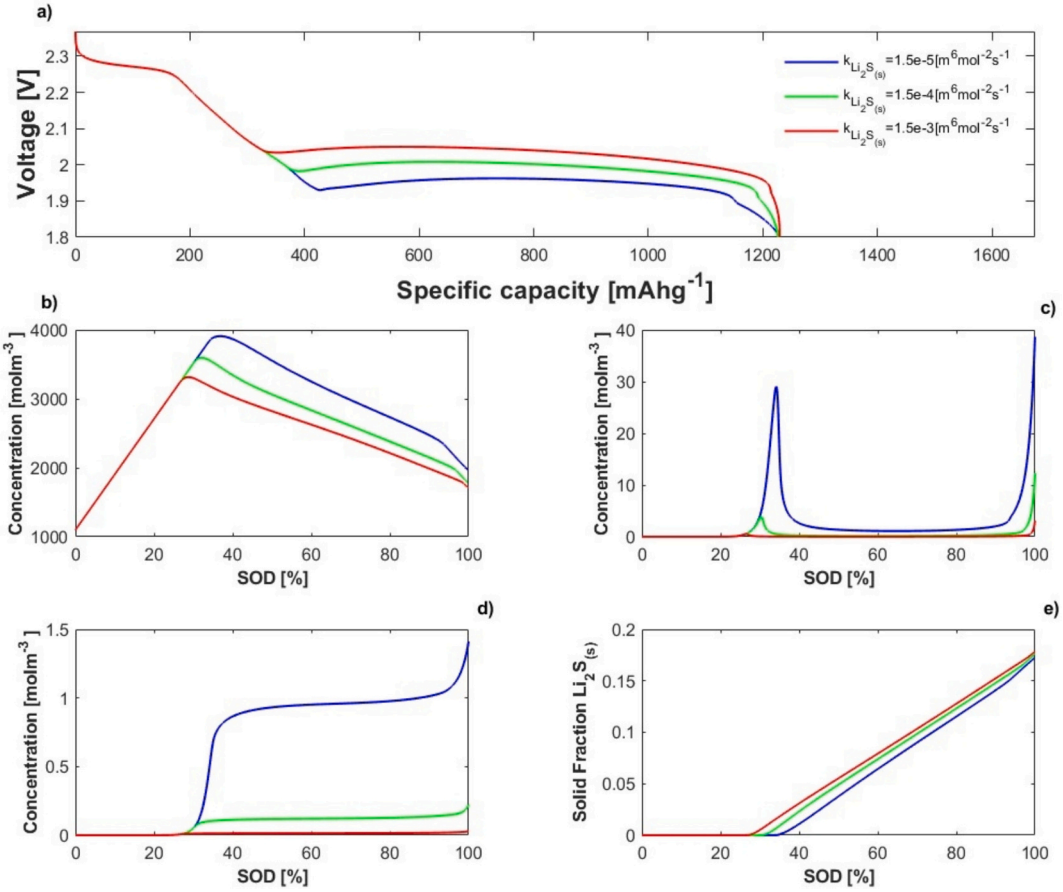

Fig. 4. Study on the effect of K_{Li2S} at high current intensity: a) Voltage vs specific capacity comparison at 1C b) Li^+ concentration inside the cathode vs SOD [%] c) S^{2-} concentration inside the cathode vs SOD[%] d) S^{2-} concentration inside the separator vs SOD[%] e) $Li_2S_{(s)}$ solid fraction vs SOD[%]For clarity, the legend is reported only in panel (a).

where also Li^+ accumulates leading to an increase of electrolyte viscosity and so inducing voltage losses, as it has been demonstrated or implemented in several studies [31,36].

After the supersaturation point, the S^{2-}concentration starts to decrease reaching a stable plateau due to the precipitation of $Li_2S_{(s)}$. This trend continues until a sudden concentration increase is observed near the end of discharge, corresponding to a second overpotential step. Overall, at 1C the accumulation of S^{2-} affects the local chemical equilibrium and results in higher activation overpotential, leading to an evident voltage drop.

3.2. Role of $Li_2S_{(s)}$ deposition at high current

To better understand the influence of $Li_2S_{(s)}$ precipitation kinetics, it was performed a parameter analysis at a fixed rate of 1C under three different kinetic conditions, expressed by the kinetic constant K_{Li_2S}. High current intensity was chosen, because as discussed and showed previously, the difference between electrochemical and faradaic reaction is more evident.

Fig. 4a shows a comparison of the voltage versus specific capacity profiles for the three case studies. Firstly, the precipitation rate does not lead to a reduction of the overall delivered capacity, however a slower reaction rate shifts the supersaturation point at higher capacity. This trend is further confirmed in Fig. 1b, which shows the evolution of $Li_2S_{(s)}$ solid phase, where the initial formation of the precipitated solid phase is significantly delayed. Specifically, a slower kinetic leads to increased accumulation of S^{2-}, which raises the voltage losses, leading to a downward shift of the second voltage plateau of over 0.1 V, in accordance with Ghaznavi et al. findings [23,32,37]. Under faster kinetic conditions, the accumulation of lithium ions in the electrolyte is minimized, reducing the viscosity of the electrolyte helping to maintain high ionic conductivity.

Lastly, the framework used for the model, differently from a pure 0D model, also allows to provide information about the separator and the concentration of active species within it, ensuring a wider understanding of the role of mass transport limitations. Fig. 4d shows the concentration of S^{2-} anions polysulfide in the separator. A slower reaction rate leads to higher concentration of S^{2-} in the porous cathode, where they are generated, causing a stronger concentration gradient. This leads discharge products stored in a non-active region, which need to be recovered during charge.

3.3. Understand cell internal resistance

As highlighted by Zhang et al. [30] and supported by specific experimental studies [26–28], electrolyte viscosity plays a critical role in determining the bulk resistivity of Li—S cells. During discharge, the electrolyte becomes increasingly saturated with polysulfides and lithium ions, which are the dominant species throughout the process. This saturation leads to a gradual increase in viscosity, resulting in a deviation from ideal solution behavior and negatively affecting ion transport properties. The most common technique used to measure the internal resistance is PEIS [24], although as it has been proven by Lacey et al. [27] also intermittent current interruption, (ICI), can potentially provide comparable results. However, as discussed by Lacey himself, this technique is affected by the variability associated with the choice of the

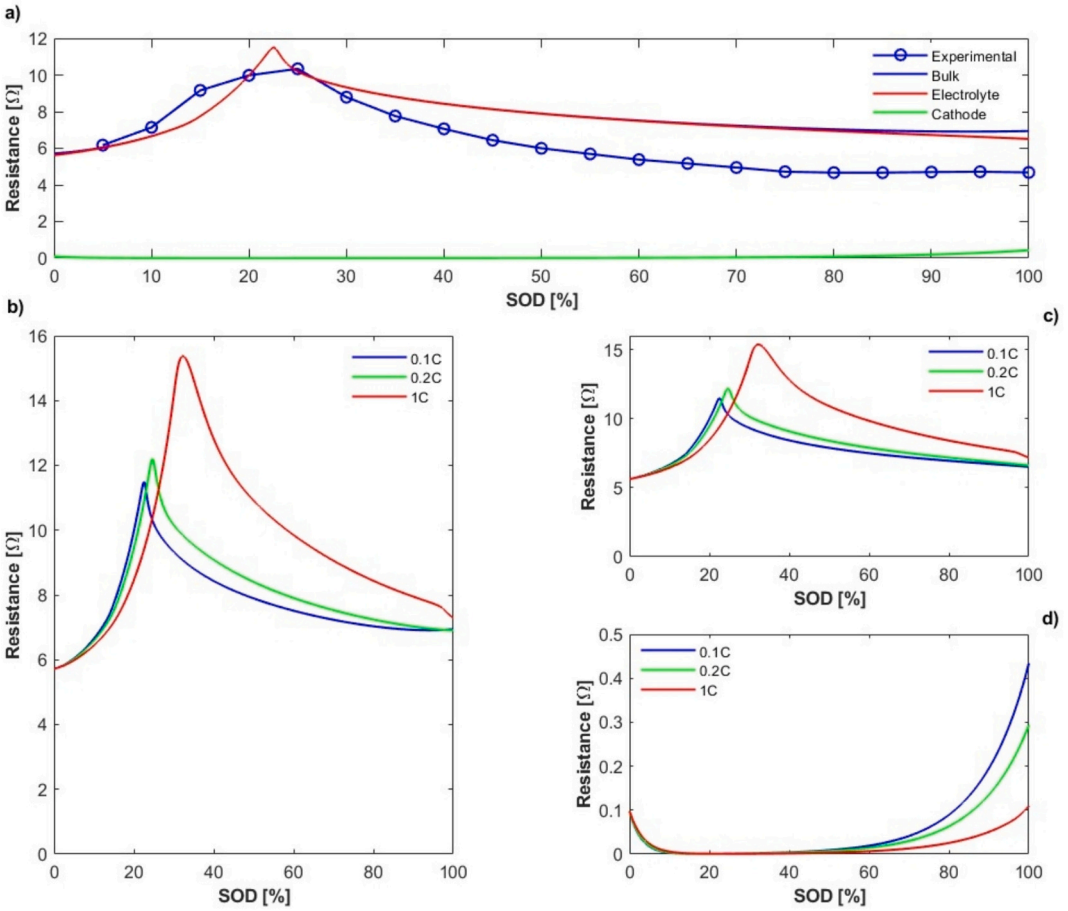

Fig. 5. Study on the effect of the C-rate on the internal resistance: a) Experimental vs modelling contribution at 0.1C b) Internal resistance vs SOD [%] for 3 different current intensity c) Electrolyte ionic resistance contribution vs SOD[%] d) Cathode electric resistance contribution vs SOD[%].

time window used for linear regression, therefore introducing relevant uncertainty in the interpretation of the results. For this reason, a more established methodology was preferred, not only in the Lithium Sulfur field, but in electrochemistry in general. Nevertheless, the trends predicted by ICI are also reported in the Supporting Information and compared with the one obtained using PEIS. Overall, the internal resistance can be simplified as the contribution coming from the ionic and electronic resistance, which in the model has been associated with the electrolyte and the cathode, respectively.

Despite its significance, many electrochemical models tend to underestimate or oversimplify the electronic insulation properties of sulfur and $Li_2S_{(s)}$, focusing mostly on the impact of electrolyte ionic conductivity as source of voltage losses. However, the insulating nature of the precipitated species is a key challenge for the future development of Li—S batteries. In the framework used for the model, as reported in eq. 23, the electrical conductivity of the porous cathode was expressed as average of the electrical properties of each solid fraction present inside. During discharge the electrical properties of the cathode changes due to dissolution and precipitation process, which involves highly insulating species. By this way, it is possible to understand the impact of the C-rate on the cathode electric conductivity.

Experimental data showed in Fig. 5, confirm a stabilization in the internal cell resistance during discharge, even though the lithium-ion concentration decreases significantly due to Li_2S precipitation. This can be explained by the progressive deposition of $Li_2S_{(s)}$on the conductive carbon structure, which decreases the overall electronic conductivity of the working electrode. This reduced conductivity counteracts the reduction of viscosity and contributes to the observed stabilization of internal resistance.

To further investigate this behavior, the dependence of cell resistivity on C-rate was also analyzed. Consistent with Zhang's findings [28], resistivity increases with higher current rates, which also impacts the position of the peak, that is slightly shifted towards higher SOD ([%]). As previously discussed, the primary driver of this trend is the electrolyte viscosity, which rises due to rapid polysulfide accumulation, indeed the contribution linked to the ionic conductivity almost overlap with the total resistivity. Additionally, at higher currents, the rate of Li^+ generation at the anode overcome the rate of $Li_2S_{(s)}$precipitation at the cathode, leading to accumulation of lithium ions in the electrolyte and further increasing resistivity. This is corroborated by the evolution of cathode resistivity shown in Fig. 4, where slower discharge rates allow for a more homogenous and complete $Li_2S_{(s)}$ deposition, in agreement with Zhang et al. [30]. This leads to a higher solid-phase volume fraction of insulating $Li_2S_{(s)}$, ultimately resulting in increased bulk resistivity at the end of discharge.

Overall, the model provides an useful tool to understand the role of $Li_2S_{(s)}$ precipitation rate and its relationship with the current rate on the overall internal resistance. As it was showed the effect is doubles and in contradiction, at high current the over concentration of dissolved species leads to a peak in the electrolyte viscosity, however at the same time, specially at the end of discharge, lower current intensity leads to higher accumulation of insulating $Li_2S_{(s)}$.

4. Conclusion

The results here presented proved that the modelling framework

used in this work provides a comprehensive description of the interplay between the several interconnected kinetics within Li—S batteries. The model highlight how the limited kinetics of polysulfide transport is responsible for the limited sulfur utilization at high discharge currents. The difference in delivered capacity when increasing the current rate from 0.1C to 1C exceeds 250[mAhg^{-1}], corresponding to more than 10% of the total theoretical capacity. By simultaneously tracking the evolution of active species concentrations in both the separator and the cathode, the adopted model framework allows to link the reduction of sulfur utilization with the residual concentration of intermediate polysulfides, as S_4^{2-}, at the end of discharge in the separator, that under 1C current rate is nearly five times higher than that obtained at 0.1C and more than twice that at 0.2C. These results were achieved without implementing any PDE and considering only the contribution of Fickian diffusion generated by concentration gradient, and therefore neglecting the electrolyte effect. While the first voltage plateau remains relatively unaffected, the second plateau suffers from pronounced capacity loss, due to the inability of polysulfides to redistribute efficiently between the cathode and the separator. Furthermore, the study demonstrates that the precipitation kinetics of $Li_2S_{(s)}$ plays a critical role on both the voltage profile and the internal resistance of the cell, affecting overpotential losses, phenomena reported in literature only at limited current intensity, proving that the framework used guarantee high flexibility towards different conditions. The model here discussed shows, with increasing current density, a shift of the peak of the system internal resistance, which can be reached at almost half of the SOD([%]). Due to the kinetic mismatch between $Li_2S_{(s)}$ deposition and electrochemical activity, this behavior may lead to an increase in internal resistance from slightly above 11[Ω] up to almost 16[Ω], corresponding to an increase of nearly 50%. For future development and optimization in the Li—S field, it is crucial to address the $Li_2S_{(s)}$ deposition process, as highlighted by the model. The model here presented provides a different approach to understand the role of the internal resistance of the cell and its different contribution, highlighting a duality between cathode and electrolyte. Moreover, the flexibility of the framework makes the P1D model discussed here a valuable tool for combined experimental and simulation-based studies, in a simple and less expensive approach.

Overall, the framework used for the model has been proved a valid tool to provide a wider understanding on the role of limited kinetics of diffusion and precipitation, and its consequences on the electrochemical performance of Li—S cells.

CRediT authorship contribution statement

Tommaso Filippo Lupatelli: Writing – review & editing, Writing – original draft, Software, Investigation, Data curation, Conceptualization. **Massimo Santarelli:** Writing – review & editing, Visualization, Supervision. **Silvia Bodoardo:** Supervision, Resources, Project administration, Funding acquisition. **Daniele Versaci:** Visualization, Validation, Methodology, Conceptualization.

Declaration of competing interest

The authors declare that they have no known competing financial interests or personal relationships that could have appeared to influence the work reported in this paper.

Acknowledgements

T.F. Lupatelli acknowledges Stellantis - CRF (Centro Ricerche Fiat) for co-funding the Ph.D. scholarship.

This publication is part of the project PNRR-NGEU which has received funding from the MUR – DM 117/2023.

Appendix A. Supplementary data

Supplementary data to this article can be found online at https://doi.org/10.1016/j.jelechem.2026.119915.

References

[1] X. Ji, L.F. Nazar, Advances in Li–S batteries, J. Mater. Chem. 20 (2010) 9821–9826, https://doi.org/10.1039/B925751A.
[2] R. Kumar, J. Liu, J. Hwang, Y.-K. Sun, Recent research trends in Li–S batteries, J. Mater. Chem. A 6 (2018) 11582–11605, https://doi.org/10.1039/C8TA01483C.
[3] Z.M. Zhao, B.Q. Li, X.Q. Zhang, J.Q. Huang, Q. Zhang, A Perspective toward Practical Lithium–Sulfur Batteries, ACS Cent. Sci. 6 (2020) 1095–1104, https://doi.org/10.1021/acscentsci.0c00443.
[4] F.S. Feng, Z.-H. Fu, X. Chen, Q. Zhang, A review on theoretical models for lithium–sulfur battery cathodes, InfoMat 4 (2022) e12304, https://doi.org/10.1002/inf2.12304.
[5] M.R. Mori, Cathode materials for lithium sulfur battery: a review, J. Solid State Electrochem. 27 (2023) 813–839, https://doi.org/10.1007/s10008-023-05349-4.
[6] Y. Deng, J. Li, T. Li, X. Gao, C. Yuan, Life cycle assessment of lithium sulfur battery for electric vehicles, J. Power Sources 343 (2017) 284–295, https://doi.org/10.1016/j.jpowsour.2017.01.036.
[7] M. Agostini, B. Scrosati, J. Hassoun, An advanced Lithium ion sulfur battery for high energy storage, Adv. Energy Mater. 5 (2015) 1500481, https://doi.org/10.1002/aenm.201500481.
[8] S.-H. Chung, A. Manthiram, Current Status and Future Prospects of Metal–Sulfur Batteries, Adv. Mater. 31 (2019) 1901125, https://doi.org/10.1002/adma.201901125.
[9] D.A. Boyd, Sulfur and its role in modern materials science, Angew. Chem. Int. Ed. 55 (2016) 15486–15502, https://doi.org/10.1002/anie.201602684.
[10] W. Ren, W. Ma, S. Zhang, B. Tang, Recent advances in shuttle effect inhibition for lithium sulfur batteries, Energy Storage Mater. 23 (2019) 707–732, https://doi.org/10.1016/j.ensm.2019.05.005.
[11] J. Wang, H. Wang, S. Jia, Q. Zhao, Q. Zheng, Y. Ma, T. Ma, X. Li, Recent advances in inhibiting shuttle effect of polysulfide in lithium-sulfur batteries, J. Energy Storage 72 (2023) 108372, https://doi.org/10.1016/j.est.2023.108372.
[12] Y. Hu, H. Du, J. Lu, H. Zhang, S. Li, X. Du, Interface synergistic stabilization of zinc anodes via polyacrylic acid doped polyvinyl alcohol ultra-thin coating, J. Energy Storage 87 (2024) 111444, https://doi.org/10.1016/j.est.2024.111444.
[13] L. Wu, Y. Hu, X. Du, J. Lu, Z. Li, N. Cao, S. Zhang, H. Du, Movable SiO2 reinforced polymethyl methacrylate dual network coating for highly stable zinc anodes, J. Energy Storage 132 (2025) 117752, https://doi.org/10.1016/j.est.2025.117752.
[14] D.M. Brieske, A. Warnecke, D.U. Sauer, Modeling the volumetric expansion of the lithium-sulfur battery considering charge and discharge profiles, Energy Storage Mater. 55 (2023) 289–300, https://doi.org/10.1016/j.ensm.2022.11.053.
[15] R. Chen, Y. Zhou, X. Li, Nanocarbon-enabled mitigation of sulfur expansion in lithium–sulfur batteries, Energy Storage Mater. 68 (2024) 103353, https://doi.org/10.1016/j.ensm.2024.103353.
[16] R. Colombo, D. Versaci, J. Amici, F. Bella, M.L. Para, N. Garino, M. Laurenti, S. Bodoardo, C. Francia, Reduced graphene oxide embedded with ZnS nanoparticles as catalytic cathodic material for Li-S batteries, Nanomaterials 13 (2023) 2149, https://doi.org/10.3390/nano13142149.
[17] G. Li, L. Wen, D. Luo, Y.P. Deng, D. Wang, Z. Chen, 3D Porous Carbon Sheets with Multidirectional Ion Pathways for Fast and Durable Lithium–Sulfur Batteries, Adv. Energy Mater. 8 (2018) 1702381, https://doi.org/10.1002/aenm.201702381.
[18] C.D. Parke, L. Teo, D.T. Schwartz, V.R. Subramanian, Progress on continuum modeling of lithium–sulfur batteries, Sustain. Energy Fuel 5 (2021) 5946–5966, https://doi.org/10.1039/D1SE01090E.
[19] M. Wild, L. O'Neill, T. Zhang, R. Purkayastha, G. Minton, M. Marinescu, G.J. Offer, Lithium sulfur batteries, a mechanistic review, Energy Environ. Sci. 8 (2015) 3477–3494, https://doi.org/10.1039/C5EE01388G.
[20] Y.V. Mikhaylik, J.R. Akridge, Polysulfide shuttle study in the Li/S battery system, J. Electrochem. Soc. 151 (2004) A1969–A1976, https://doi.org/10.1149/1.1804812.
[21] K. Kumaresan, Y. Mikhaylik, R.E. White, A mathematical model for a lithium–sulfur cell, J. Electrochem. Soc. 155 (2008) A576, https://doi.org/10.1149/1.2937304.
[22] T. Zhang, M. Marinescu, S. Walus, G.J. Offer, Modelling transport-limited discharge capacity of lithium-sulfur cells, Electrochim. Acta 219 (2016) 502–508, https://doi.org/10.1016/j.electacta.2016.10.032.
[23] M. Ghaznavi, P. Chen, Analysis of a mathematical model of Lithium-sulfur cells part III: electrochemical reaction kinetics, transport properties and charging, Electrochim. Acta 137 (2014) 575–585, https://doi.org/10.1016/j.electacta.2014.06.033.
[24] Talian S. Drvarič, J. Moškon, R. Dominko, M. Gaberšček, The pitfalls and opportunities of impedance spectroscopy of Lithium sulfur batteries, Adv. Mater. Interfaces 9 (2022) 2101116, https://doi.org/10.1002/admi.202101116.
[25] W. Li, B. Wang, Y. Chen, Y. Deng, C.N. Markides, M. Zeng, Discharge characteristic analysis of lithium-sulfur batteries considering the discontinuous deposit and transport-limited effects, J. Clean. Prod. 436 (2024) 140719, https://doi.org/10.1016/j.jclepro.2024.140719.
[26] M.J. Lacey, K. Edström, D. Brandell, Visualising the problems with balancing lithium–sulfur batteries by "mapping" internal resistance, Chem. Commun. 51 (2015) 16502–16505, https://doi.org/10.1039/C5CC06700H.

[27] M.J. Lacey, Influence of the electrolyte on the internal resistance of Lithium−sulfur batteries studied with an intermittent current interruption method, ChemElectroChem 4 (2017) 1997–2004, https://doi.org/10.1002/celc.201700129.
[28] V.S. Kolosnitsyn, E.V. Kuzmina, S.E. Mochalov, Determination of lithium Sulphur batteries internal resistance by the pulsed method during galvanostatic cycling, J. Power Sources 252 (2014) 28–34, https://doi.org/10.1016/j.jpowsour.2013.11.099.
[29] N.A. Cañas, K.A. Friedrich, N. Wagner, B. Pascucci, R. Hiesgen, Investigation of rechargeable lithium sulfur batteries by in situ techniques, ECS Meeting Abstracts, in: 224th ECS Meeting, 2013, https://doi.org/10.1149/MA2013-02/6/376.
[30] T. Zhang, M. Marinescu, L. O'Neill, M. Wild, G. Offer, Modeling the voltage loss mechanisms in lithium–sulfur cells: the importance of electrolyte resistance and precipitation kinetics, Phys. Chem. Chem. Phys. 17 (2015) 22581–22586, https://doi.org/10.1039/C5CP03566J.
[31] Y.X. Ren, T.S. Zhao, M. Liu, P. Tan, Y.K. Zeng, Modeling of lithium-sulfur batteries incorporating the effect of Li2S precipitation, J. Power Sources 336 (2016) 115–125, https://doi.org/10.1016/j.jpowsour.2016.10.063.
[32] M. Ghaznavi, P. Chen, Sensitivity analysis of a mathematical model of lithium–sulfur cells part I: applied discharge current and cathode conductivity, J. Power Sources 257 (2014) 394–401, https://doi.org/10.1016/j.jpowsour.2013.10.135.
[33] T. Danner, G. Zhu, A.F. Hofmann, A. Latz, Modeling of nano-structured cathodes for improved lithium-sulfur batteries, Electrochim. Acta 184 (2015) 124–133, https://doi.org/10.1016/j.electacta.2015.09.143.
[34] T. Danner, A. Latz, On the influence of nucleation and growth of S8 and Li2S in lithium-sulfur batteries, Electrochim. Acta 322 (2019) 134719, https://doi.org/10.1016/j.electacta.2019.134719.
[35] V. Thangavel, K.-H. Xue, Y. Mammeri, M. Quiroga, A. Mastouri, C. Guéry, P. Johansson, M. Morcrette, A.A. Franco, A microstructurally resolved model for Li-S batteries assessing the impact of the cathode design on the discharge performance, J. Electrochem. Soc. 163 (2016) A2817, https://doi.org/10.1149/2.0051614jes.
[36] A.N. Mistry, P.P. Mukherjee, Electrolyte Transport Evolution Dynamics in Lithium–Sulfur Batteries, J. Phys. Chem. C 122 (2018) 18329–18335, https://doi.org/10.1021/acs.jpcc.8b03410.
[37] M. Ghaznavi, P. Chen, Sensitivity analysis of a mathematical model of lithium–sulfur cells: part II: precipitation reaction kinetics and sulfur content, J. Power Sources 257 (2014) 402–411, https://doi.org/10.1016/j.jpowsour.2013.12.145.